Chapter 3.

Calibration and Limitations of the Quartz Crystal Microbalance.

3.1. Introduction.

As discussed in Chapters 1 and 2, the quartz crystal microbalance (QCM) utilises the piezoelectric qualities of quartz crystals. The application of an electric field to the gold coated quartz crystals causes a shear deformation (parallel to the gold surface). The crystal can be made to resonate if an alternating electric field is applied at a particular frequency $f_0(m)$. This resonant frequency is given by the following equation:

$$f_0(m) = \frac{\sqrt{\mu_q}}{2x_q\sqrt{\rho_q}} \qquad \textbf{(3.1)}$$

where μ_q is the shear modulus of the quartz crystal (2.947×10^{11} dyne cm^{-2} for AT-cut quartz), ρ_q is the density of quartz (2.648 g cm^{-3}) and x_q is the thickness of the quartz.

Deposition of the gold (working electrode) layer dampens this resonant frequency. This resonant frequency is viscously damped when the gold quartz crystal electrode is placed in the aqueous electrolyte solution. Also rigid attachment of mass to the gold surface will further dampen this frequency. The Sauerbrey equation [1] relates the dampening of frequency (Δf_0) to the change in surface attached mass (Δm), assuming a thin, uniform, rigidly attached mass. Following is a derivation of the Sauerbrey equation based on a similar method for deriving a different form of the Sauerbrey equation [2]. In order to derive this equation the following simple relation is required:

$$M = \frac{m}{A} = x_{\mathrm{q}} \rho_{\mathrm{q}} \tag{3.2}$$

where M is the mass of the quartz crystal per unit area, m is the total mass of the quartz crystal, A is the area of the quartz crystal.

Now Equation 3.1. can be combined with equation 3.2 to give:

$$f_0(M) = \frac{\sqrt{\mu_{\mathrm{q}} \rho_{\mathrm{q}}}}{2M} \tag{3.3}$$

The addition of mass (per unit area) ΔM causes a change in resonant frequency Δf_0:

$$f_0(M) + \Delta f_0 = \frac{\sqrt{\mu_{\mathrm{q}} \rho_{\mathrm{q}}}}{2(\mathrm{M} + \Delta M)} \tag{3.4}$$

Now, combining equation 3.3. with equation 3.4.:

$$\Delta f_0 = \frac{\sqrt{\mu_{\mathrm{q}} \rho_{\mathrm{q}}}}{2(\mathrm{M} + \Delta M)} - \frac{\sqrt{\mu_q \rho_q}}{2M} \tag{3.5}$$

$$= \frac{-\sqrt{\mu_q \rho_q}\,\Delta M}{2(M + \Delta M)M}$$

$$= \frac{-\sqrt{\mu_q \rho_q}\,\Delta M}{2M^2(1 + \frac{\Delta M}{M})} \tag{3.6}$$

Now combining equation 3.6. with equation 3.3.:

$$\Delta f_0 = \frac{-f_0(M)\Delta M}{M(1+\frac{\Delta M}{M})} \qquad \textbf{(3.7)}$$

For a thin deposit, where $\Delta M << M$ equation 3.7 becomes (when combined with equation 3.2.):

$$\Delta f_0 = \frac{-f_0(0)\Delta M}{M} = \frac{-f_0(0)\Delta m}{A x_q \rho_q} \qquad \textbf{(3.8)}$$

Note: $f_0(0)$ is the resonant frequency (with no attached mass).

So this equation is the Sauerbrey equation:

$$\Delta f_0 = -\left(\frac{f_0(0)}{\mathrm{A}\ x_q \rho_q}\right)\Delta m = -S\Delta m \qquad \textbf{(3.9)}$$

where Δm is the change in surface mass, A is the piezoelectrically active area and S is the Sauerbrey constant.

For a particular resonant frequency crystal (eg 10 MHz) the Sauerbrey constant is independent of any solution chemistry. This is because the Sauerbrey constant depends on well known physical constants. Consequently no calibration of the instrument (which uses the Sauerbrey equation to output mass data) is required. However, the validity of the Sauerbrey equation to thick and or non uniform

deposits of mass is debatable. In this chapter, the use of metal deposition processes to test the capabilities of the instrument and the applicability of the Sauerbrey equation are described.

Massograms introduced in Chapter 2, are presented for the QCM data in which the mass is differentiated with respect to time (J) and plotted versus potential. The massogram allows instantaneous mass data to be directly related to current (dQ/dt), rather than the accumulation of mass which relates directly to charge. In this chapter, massograms are used to examine the suitability of various metal deposition processes for QCM calibration.

3.2. Experimental Section.

3.2.1. Chemicals. Lead acetate trihydrate (99.5%, AR grade), cupric sulphate pentahydrate (99.5%, AR grade), sodium acetate anhydrous, acetic acid (99.9%) and concentrated nitric acid (69-71% in water) were all obtained from BDH Chemicals Ltd. Potassium nitrate (99.5%) was obtained from UNIVAR. Water from a MilliQ Reagant System (>10 MΩ cm resistivity) was used for preparation of all the aqueous electrolyte solutions.

3.2.2. Electrochemical Apparatus and Conditions.

Voltammograms and mass balance measurements were obtained using equipment described in Chapter 2, Experimental Section.

All experiments were carried out at ambient temperatures ($20 \pm 2\ ^{o}C$), and all solutions were deoxygenated using high purity nitrogen unless otherwise stated. The reference half-cell was Ag/AgCl in 3M KCl. Working electrodes were 13-mm diameter *AT*-cut α-quartz crystals (Bright Star Crystals, Rowville, Victoria, Australia). These had gold disks (5.0 mm diameter) vapour deposited on each side, and resonated in air at 10 ± 0.05 MHz. Before each experiment, electrodes were cleaned using a 50:50 mixture of concentrated nitric acid and water.

3.3. Results and Discussion.

3.3.1. Calibration of the instrument.

As discussed in the introduction, if the Sauerbrey equation is valid, the quartz crystal microbalance technically does not need to be calibrated. However, it is always sound practice to ensure that the instrument is functioning properly and is reporting accurate (mass) data and also to test the capabilities of the instrument. Consequently, in Section 3.3.1., the validity of the Sauerbrey equation is being tested, particularly for cases where deposits are thick and non uniform.

The Elchema manual [3] suggests that the EQCM calibration be performed using copper deposition (in 0.1M HNO_3(aq)), while other workers [4-5,1] have used silver to calibrate the EQCM. In this chapter, the problems associated with these

systems are discussed. The use of lead deposition is explored and consequently recommended as a superior calibrant to copper and silver.

3.3.1.1. Copper deposition.

The metal deposition system recommended by Elchema [3] for calibration of the instrument is the electro-deposition of copper [6] via the reduction of 10 mM $CuSO_4$ in 0.1M HNO_3 (aq). This system is complicated by overlap of the metal reduction process with the hydrogen evolution reaction as illustrated in Chapter 2 (see Figure 2.3.). Using massograms it was possible to separate the metal deposition process from the hydrogen evolution reaction. Figure 2.3.a) shows the cyclic voltammetry of a 10mM $CuSO_4$ in 0.1M HNO_3(aq) at 100 mV s^{-1} on a gold quartz crystal. There is a large background reductive current due to the hydrogen evolution reaction:

$$2H^+(aq) \xrightarrow{+2e^-} H_2(g) \qquad \textbf{(3.10)}$$

The underlying metal deposition process is extracted from the data using a massogram plot (Figure 2.3. b). This plot reveals a small diffusion limited peak which is indistinguishable from the hydrogen evolution reaction in the standard cyclic voltammogram. This peak is due to the process:

$$Cu^{2+}(aq) \xrightarrow{+2e^-} Cu(solid) \qquad \textbf{(3.11)}$$

Thus, calibration of the EQCM instrument using the reduction peak in 0.1M HNO_3(aq) is problematic. There is also a slight overlap of the hydrogen evolution reaction with the metal oxidation / dissolution process, which results in a shift in the crossover point (where the current passes through zero on the reverse scan). This crossover point has been shown [7] to be the position of the reversible potential (E^0), if there are no extraneous currents. The shift in crossover point is made more dramatic when solutions of lower pH are used (Figure 2.4). The lower the pH the more positive the potential for the hydrogen evolution reaction. This can be explained by the Nernst equation [8]:

$$E_{red} = E^0_{red} - \frac{0.00019841T}{n} \log_{10} \frac{(a_p)^x}{(a_r)^y} \qquad \textbf{(3.12)}$$

where T is the temperature (Kelvin), n is the number of electrons, a_p is the activity of the product, a_r is the activity of the reactant, and x and y are the coefficients of the products and reactants respectively.

For the hydrogen evolution reaction the equation becomes at 25^0C:

$$E_{red} = E^0_{red} - \frac{0.05916}{n} \log_{10} \frac{|H_2(gas)|}{|H^+(aq)|^2} \qquad \textbf{(3.13)}$$

According to this equation, the higher the concentration of H^+ (i.e. lower pH) the more positive the reversible potential becomes. Of course, the hydrogen evolution process is kinetically rather than thermodynamically controlled, but experimentally it has been shown that this kinetic effect influences the process in a systematic manner.

At higher pH (0.01M HNO_3[aq]), the copper reduction is now well removed from the hydrogen evolution reaction. However, in this case, the oxidation/dissolution process yields excessively large massogram peaks (Figure 3.1). The oxidation massogram peak is much higher than its voltammetric counterpart. Cu^+ is now stable in the higher pH regime so the reoxidation of Cu(s) results in a mixture of Cu^+ and Cu^{2+} redox states. This is illustrated by the following equations:

$$Cu^{2+}(aq) \xrightarrow{+2e^-} Cu(solid) \qquad \textbf{(3.14)}$$

$$Cu(solid) \begin{cases} \xrightarrow{+e^-} Cu^+(aq) \\ \xrightarrow{+2e^-} Cu^{2+}(aq) \end{cases} \qquad \textbf{(3.15)}$$

Therefore the current is less than expected for the two-electron reduction process. The current will be somewhere intermediate between one and two electrons as a mixture of Cu^+ and Cu^{2+} is formed.

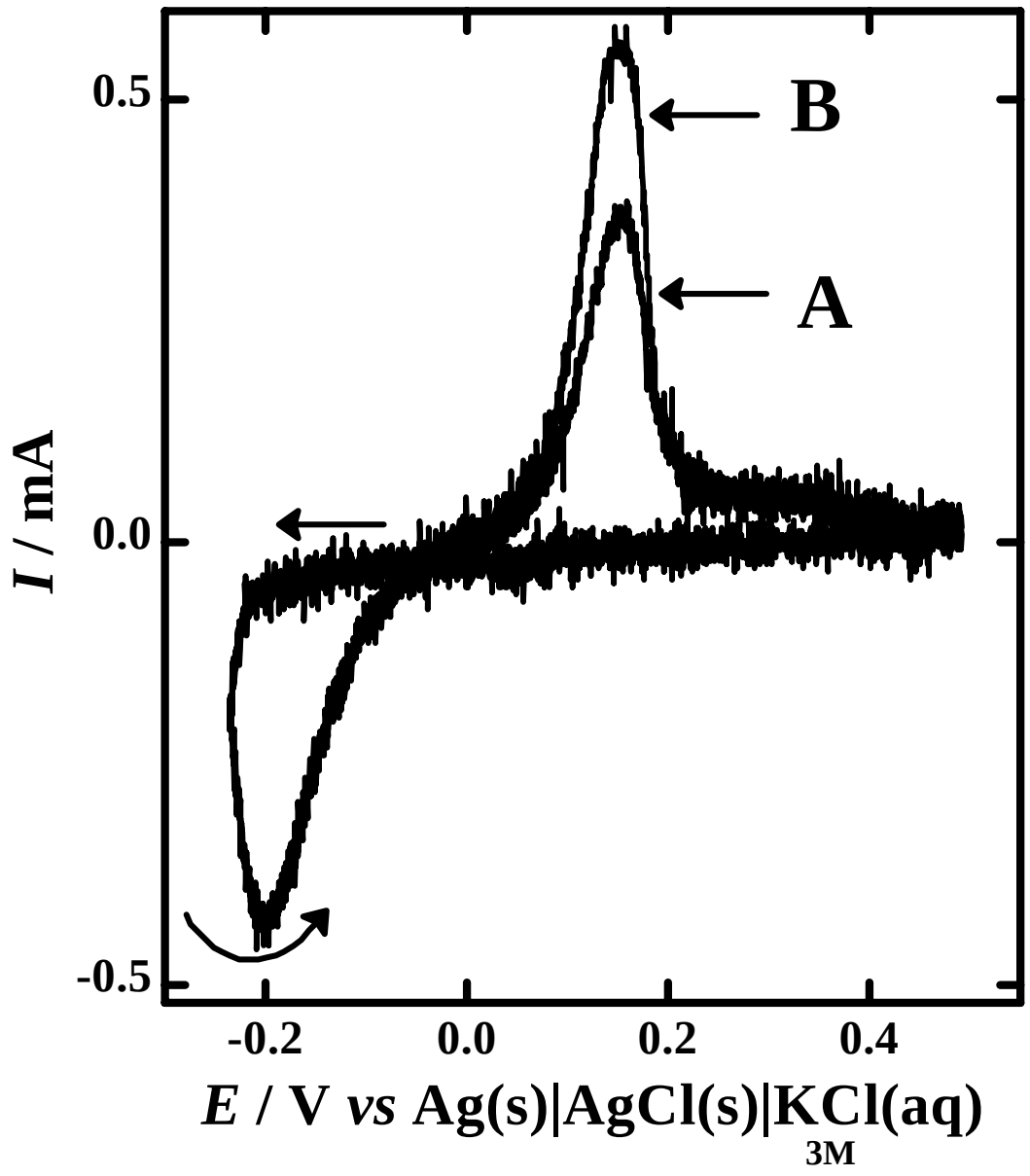

Figure 3.1. a) Voltammogram of 10 mM $CuSO_4.5H_2O$ / 0.01M HNO_3(aq)/2.5M KNO_3(aq) at 100 mV s^{-1}. Potential switched at the foot of the reduction wave. b) Massogram.

In summary, the copper reduction process is far from ideal as a calibrant for the quartz crystal microbalance. At pH below 1, the process overlaps with the hydrogen evolution reaction and at higher pH, the Cu(1) oxidation state becomes stable, complicating the comparison of the oxidative current peak with the corresponding massogram.

3.3.1.2. Silver deposition.

In many QCM studies reported in the literature [4-5,1], silver was used to calibrate the quartz crystal microbalance. The reduction process is shown below:

$$Ag^{+}(aq) \xrightarrow{+e^{-}} Ag(solid) \qquad \textbf{(3.16)}$$

However, it has been discovered that silver deposited on the gold surface cannot be fully removed [9]. Therefore, residual silver will interfere with subsequent experiments. As discussed later, lead is found to be removed fully from the electrode in acetate media. For this reason lead is considered a better calibrant than silver. There is also the question of stability of the silver deposits. Silver tends to form large crystals attached to the electrode via small necks. Some results tended to suggest that some of these crystals may be dislodged from the electrode due to the vibrational nature of the experiment.

3.3.1.3. Lead deposition.

The reduction of lead in 0.1M acetic acid/0.1 sodium acetate solution is a significantly better system for calibration of the EQCM instrument. The reduction of lead is described by the equation:

$$Pb^{2+}(aq) \xrightarrow{+2e^-} Pb(s) \qquad \textbf{(3.17)}$$

At pH 5, in a buffered solution, the reduction process is well removed from the hydrogen evolution reaction, Pb^+ is not a stable oxidation state, oxide formation is avoided, and the lead is removed fully and reversibly from the electrode.

Thus using Faraday's law, the charge can be related to the mass change using the following equation:

$$Q_{dep} = \frac{2F}{m_{w(dep)}} * \Delta m_{dep} \qquad \textbf{(3.18)}$$

where Q_{dep} = the charge deposited [C], F = faraday's constant [C.mol^{-1}], $m_{w(dep)}$ is the molecular weight of lead [g.mol^{-1}] and Δm_{dep} is the change in mass deposited on the quartz crystal [g].

Alternatively, by differentiating both sides:

$$I = \frac{2F}{m_{w(dep)}} * \frac{d(\Delta m)}{dt} \qquad \textbf{(3.19)}$$

where I = current (A) and t = time (s).

The validity of the Sauerbrey equation can now be tested using either equation (3.18) or (3.19). The first approach using the charge (integrated current) can be illustrated using an 8mM solution of lead acetate in 0.1M acetic acid/0.1M sodium acetate buffer solution. The voltammetric data was integrated using a Fortran program (see Appendix A). These experiments involved stepping the voltage gradually into the reduction process in order to control the amount of reaction. Experiments were repeated three times using different intervals.

Figure 3.2., shows the comparison of mass data with the integrated current (charge) data. The mass has been scaled to the charge using equation (3.18). It can be seen that at low depositions the mass is a little too low and at larger depositions the mass is significantly too high. Figure 3.3, shows a plot of $\frac{\Delta m_{dep}}{Q_{dep}} * \frac{2F}{m_{w(dep)}}$, which has been referred to as the calibration constant. If the Saubrey equation is valid, the value of this constant will be unity. Figure 3.3., shows that for small depositions, the constant is below unity. This is because correction for background current has not been undertaken. At these low depositions, background current is significant. Mid depositions give a reasonably accurate (within 10% error) calculation of molecular weight. However, at high depositions the calibration constant is above unity but appears to asymptote at a value which contains a 12%

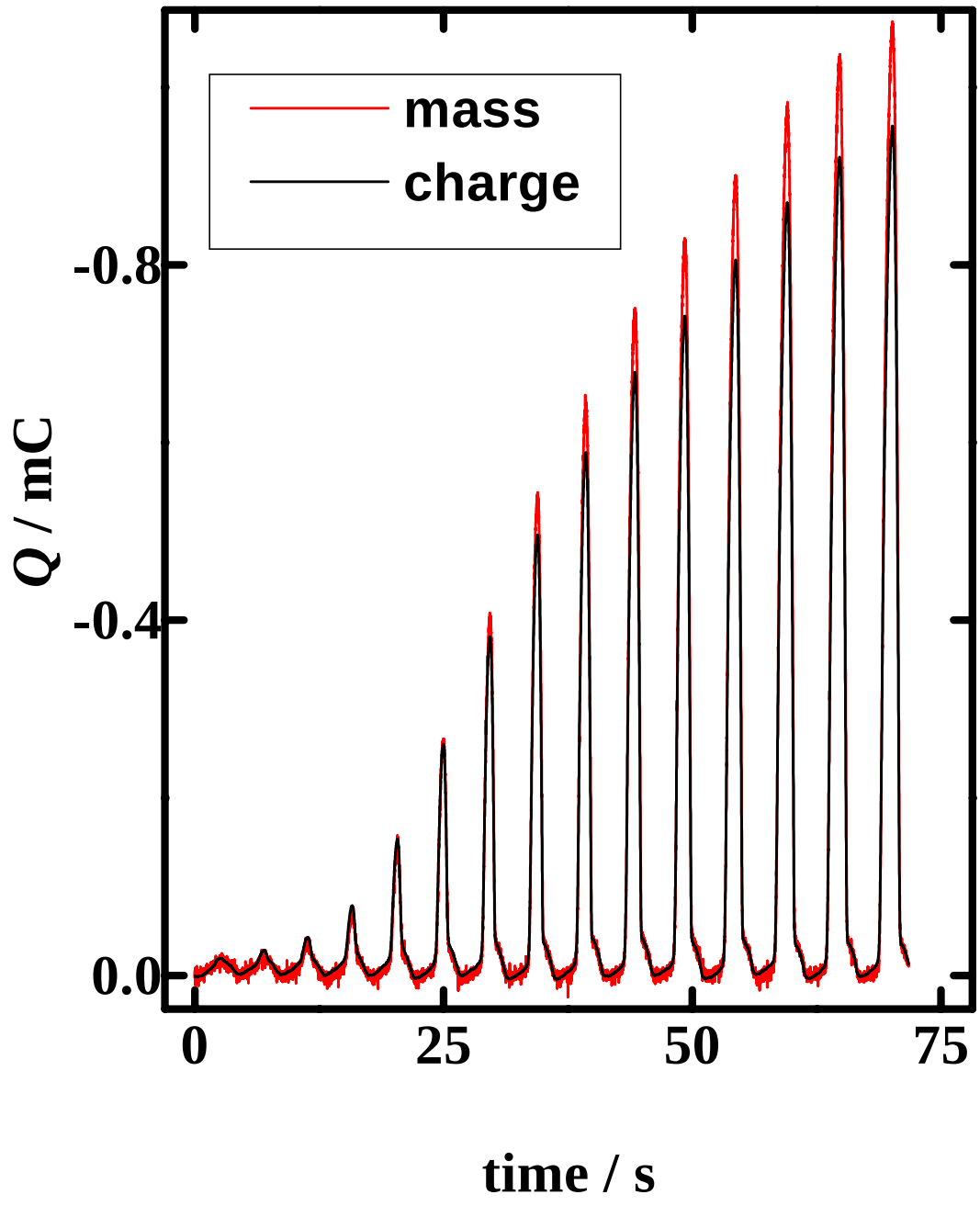

Figure 3.2. Comparison of charge (black) with mass scaled to Pb^{2+} (red) for the voltammetric cycling of 8 mM $Pb(acetate)_2$ in 0.1M acetic acid/0.1M sodium acetate (aq) on a gold quartz crystal at a scan rate of 100 mV s^{-1} (stepping progressively further into the reduction wave). Note: deviation from unity at high loading

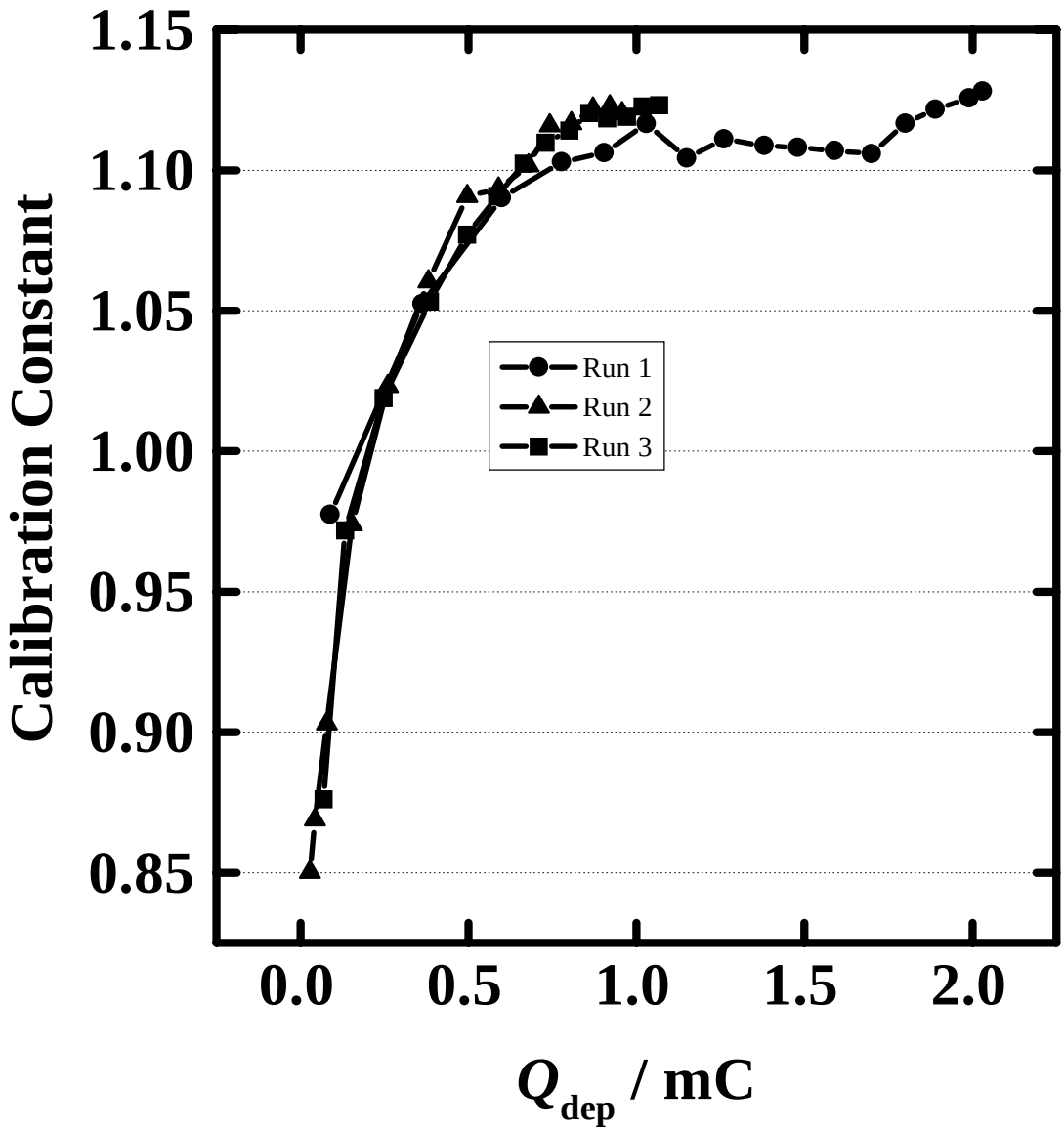

Figure 3.3. Calibration curve for Pb^{2+} reduction [8 mM $Pb(acetate)_2$] in 0.1M acetic acid / 0.1M sodium acetate on a gold quartz crystal at 100 mV s^{-1}.

error. The origin of this error is unclear. The breakdown in linearity could be due to the fact that the Sauerbrey equation only applies to a thin rigid film.

The second approach using equation (3.19) is illustrated in Figure 3.4 using the massogram plot. Again a departure from linearity is observed at large depositions. The dotted curve (the massogram) fits well at low current but departs from a linear correlation at higher currents. Again, it is most likely this departure is due to a breakdown in the Sauerbrey relation, which applies only to thin, uniform, rigid films. Thus there are several artifacts which may result in significant errors in QCM measurements of absolute mass, so that caution is required if such measurements are to be undertaken.

Figure 3.5., shows a more dilute solution (1mM) of lead in 0.1M acetic acid/0.1M sodium acetate. At this concentration the curves match well. There is a slight discrepancy due to background current but this amounts to less than a 10% error. The reduction peak at –0.31V and the oxidation peaks at –0.23V and 0.02V are due to underpotential deposition (UPD) [5,10-12] and dissolution respectively, whereas the reduction peak at –0.58V and the oxidation peak at –0.31V is due to bulk deposition and dissolution respectively. Underpotential depositions tend to be of monolayer quantities. Thus the background currents and underpotential deposition are of concern for measurements of lead concentrations this low.

Based on these results it is recommended to use around 8 mM lead acetate in 0.1M acetic acid/0.1M sodium acetate buffer solution to calibrate the instrument. A

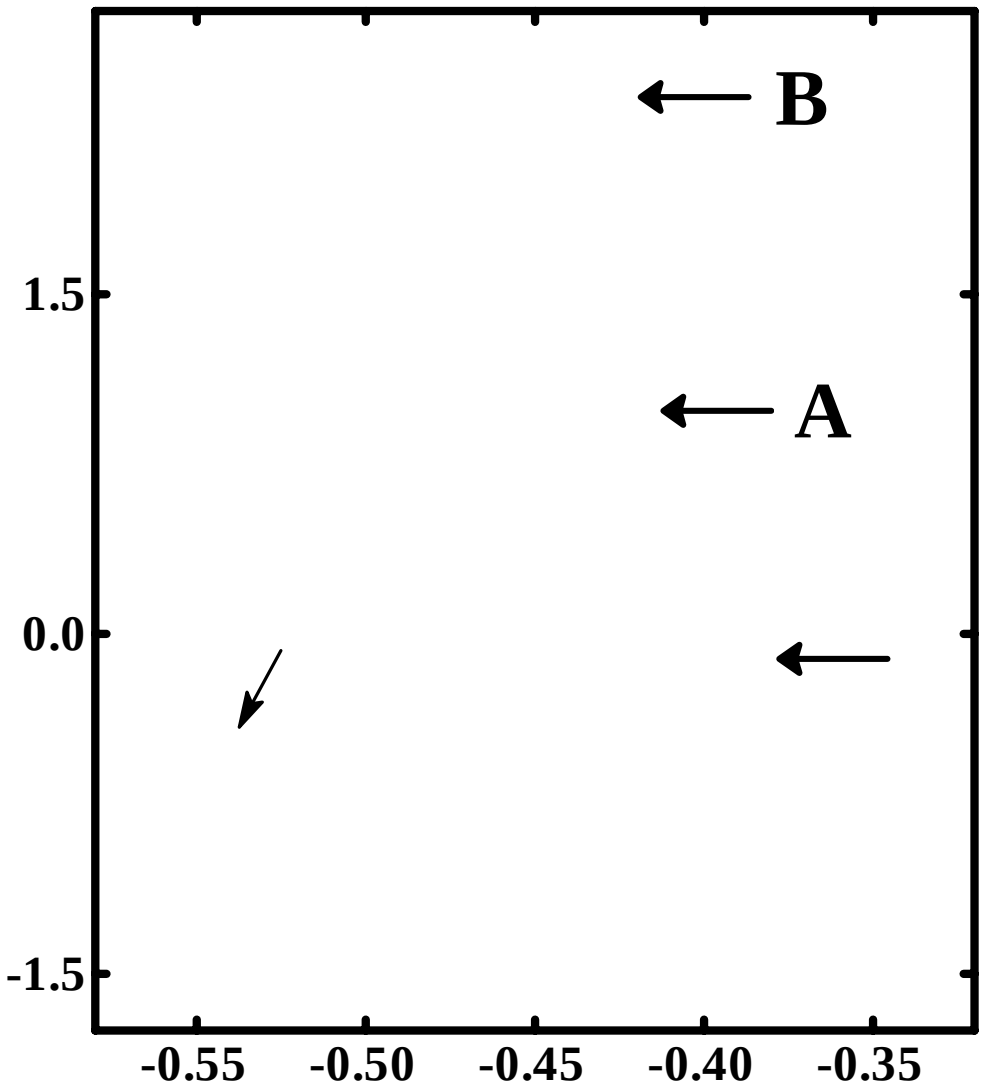

Figure 3.4. a) Voltammogram of 8 mM Pb(acetate)$_2$ in 0.1M acetic acid / 0.1M sodium acetate (aq) on a gold quartz crystal at a scan rate of 100 mV s^{-1}.

b) Dashed line is the massogram scaled to Pb^{2+}. Note deviation at high loading.

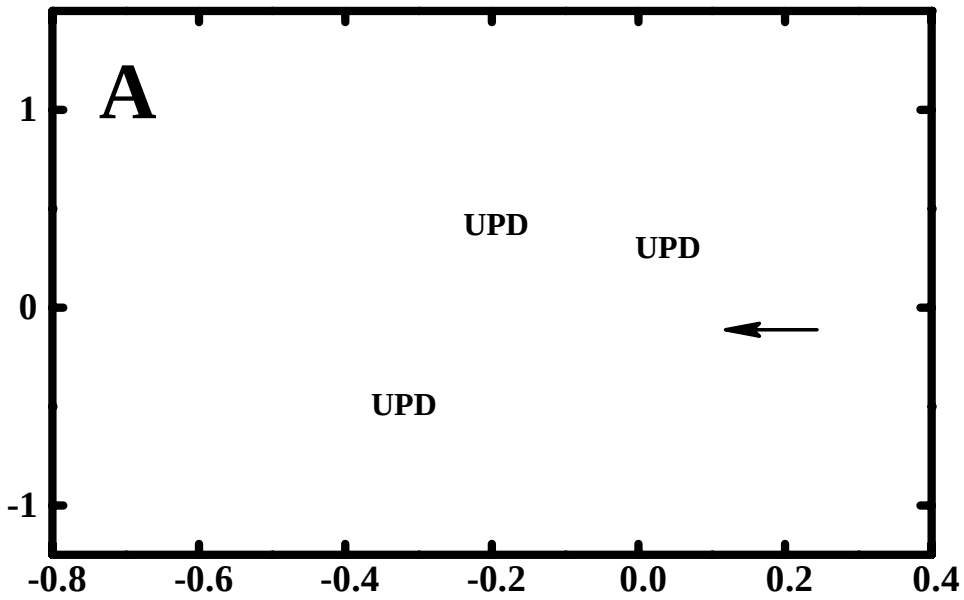

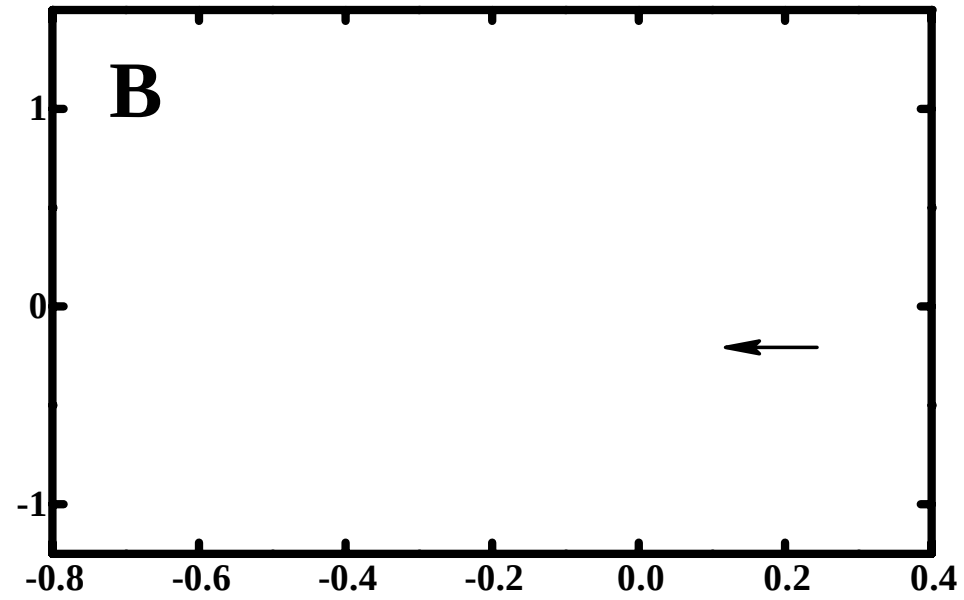

Figure 3.5. a) Voltammogram of 1mM Pb(acetate)$_2$ in 0.1M acetic acid / 0.1M sodium acetate (aq) on a gold quartz crystal at a scan rate of 100 mV s^{-1}. b) "massogram" scaled to Pb^{2+}.

mass deposition of 0.3 μg is optimum. Because lower depositions create problems with background currents that need to be subtracted and larger depositions create problems due to the breakdown of the Sauerbrey equation for thick deposits. Voltammetry requires reversing the reductive sweep prematurely at the foot of the wave to limit the amount of reaction. Deviation of less than 10% from the Sauerbrey equation are expected under these recommended conditions.

3.3.2. Limitations of Instrumentation.

3.3.2.1. Spatial Distribution of Sensitivity.

In cases where there is a non-uniform distribution of mass on the quartz crystal, problems will arise due to a spatial distribution of sensitivity. In other words the frequency change is dependent on the location of the deposit. This spatial distribution of sensitivity using deposition of copper was studied by Hillier and Ward [13] with a Scannning Electrochemical Microscope. A mass sensitivity profile was obtained by measuring the frequency change for identical deposits at various locations of the electrode. Figure 3.6., shows the sensitivity profile measured. This spatial distribution of sensitivity will arise as a problem when reducing TCNQ in 0.05M CsCl as described in Chapter 4.

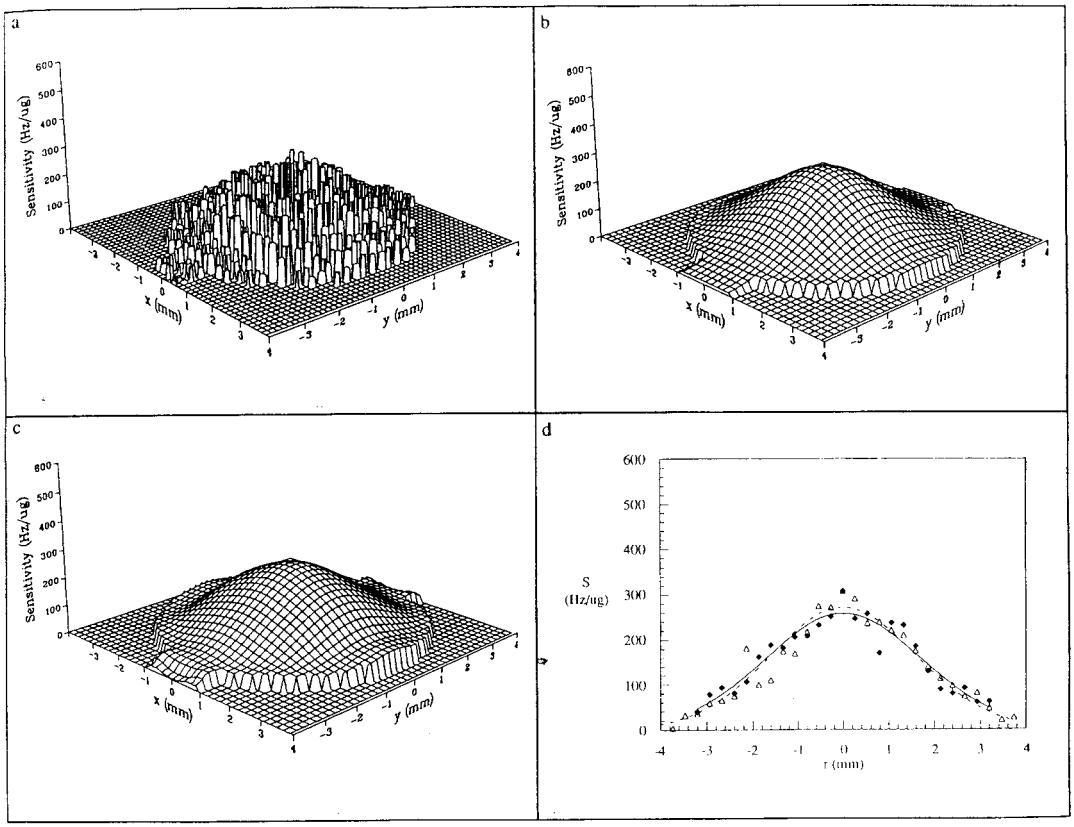

Figure 3.6. Determination of the sensitivity distribution for the 5 MHz AT-cut plano-plano quartz crystal microbalance in 20 mM $CuSO_4$ solution: a) raw data, b) Guassian curve-fit, c) smoothed data, d) line plot (triangle – parallel, diamond – perpendicular) [13]

3.3.2.2. Leakage Current.

Additional problems arise if the solution leaks through the o-ring (see Figure 1.8) onto the other side of the crystal. Such leakage manifests itself as a sloping capacitive background current as there is a short circuit through the resistive solution. A measurement is shown in Figure 3.7, in which the cell begins to leak mid-experiment which is evidenced by the onset of an enhanced capacitive background current.

3.3.2.3. Ohmic (IR) drop.

Through the course of these studies, two cell designs were used for the measurements. The first is the simple setup based on the Elchema cell setup (illustrated in Figure 1.8). This designed involved a neck attached to the cell leading to the working electrode. This neck allowed a clamp to be placed around the quartz crystal holding it in place between two o-rings. Unfortunately this neck prohibits close placement of the reference salt bridge and the working electrode. This design is suitable when measuring small currents where the IR drop is not significant. However, for studies of TCNQ and TTF (Chapter 4), which involve large currents being passed at rapid rates, close proximity of the reference electrode and working electrode is required to minimise the substantial IR drop [14]. Thus a new cell design is necessitated.

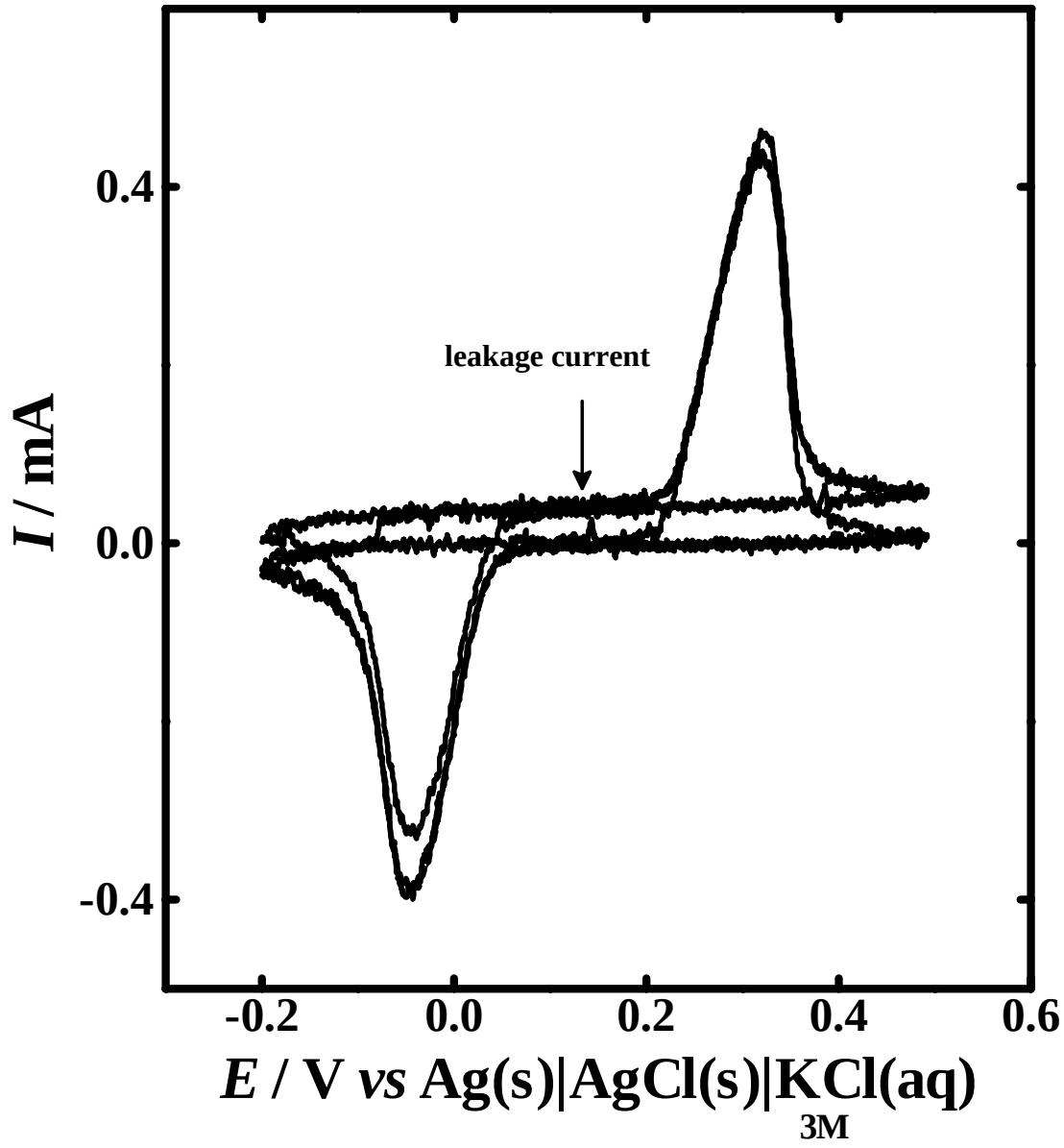

Figure 3.7. Voltammogram of TCNQ rubbed onto gold quartz crystal in 0.1M KCl(aq) [scan rate of 100 mV s^{-1}]. First scan exhibits no leakage current but subsequent scans exhibit a capacitative component due to leakage of the cell occuring.

To minimise the IR drop problem, a new cell was designed which has a less pronounced neck and an external mount holding the quartz crystal in place. In addition, the reference electrode was placed in a Luggin probe which could be adjusted horizontally so that it could be positioned as close as possible to the working electrode. This design is illustrated in Figure 3.8. The effect of IR drop on the voltammetry is illustrated in Figure 3.9. The solid line shows the voltammetry with Luggin capillary as close as possible to the working electrode (within millimetres). The peaks are sharp and narrow. The dotted line in Figure 3.9., shows the voltammetry with the Luggin tip 1 cm from the working electrode. In the presence of IR drop, the peaks decreased in height and are broadened. From Ohms Law it is known that I = V/R, so the maximum current that can be passed is limited by the slope 1/R. The voltammetric curve is linear when it first hits the IR barrier. Consequently, voltammetry using the first design is severely distorted when large currents are passed. Thus, although the Elchema cell design is far easier to assemble and less prone to leakage, voltammetry using this first design is severely distorted when large currents are passed; the second cell design (Figure 3.8) is much better suited for measurements of such high currents.

3.3.2.4. Scan Rate Limitation.

Because of the time required to locate the resonant frequency, there is an upper limitation on the scan rate that can be used. The Elchema instruction manual suggests limiting the scan rate to 600 mV s^{-1}. However, scans of 1000 mV s^{-1} of TTF in KBr were possible without distortion due to the time limitation. Figure 3.10

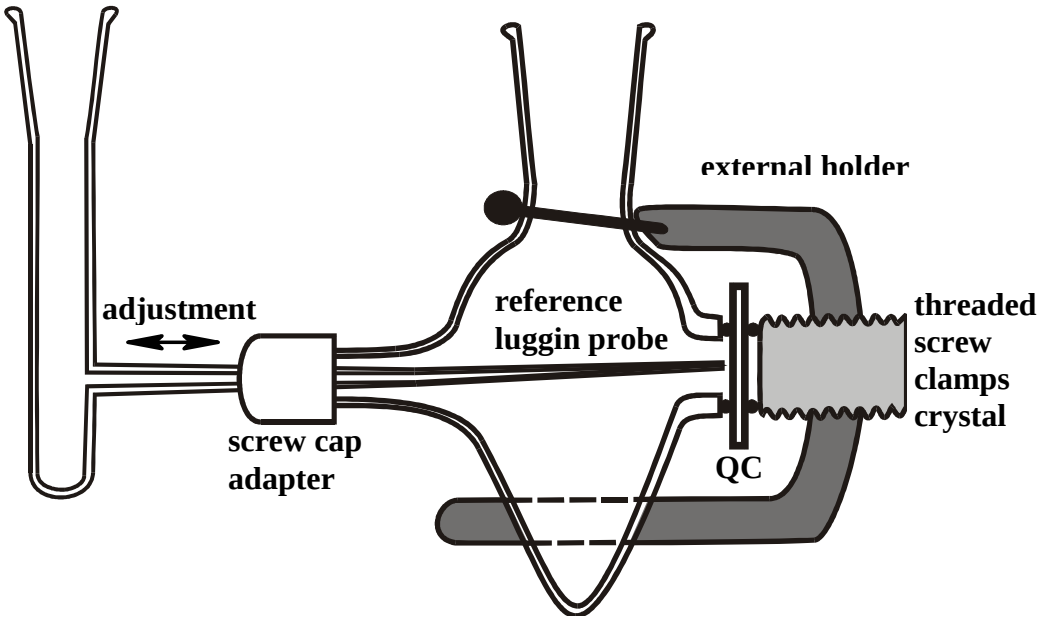

Figure 3.8. New cell design for the Quartz Crystal Microbalance, in which the quartz crystal is held in place by a external holder and the reference luggin probe is horizontal adjustable in order to place it as close as possible to the working electrode (within 1 mm).

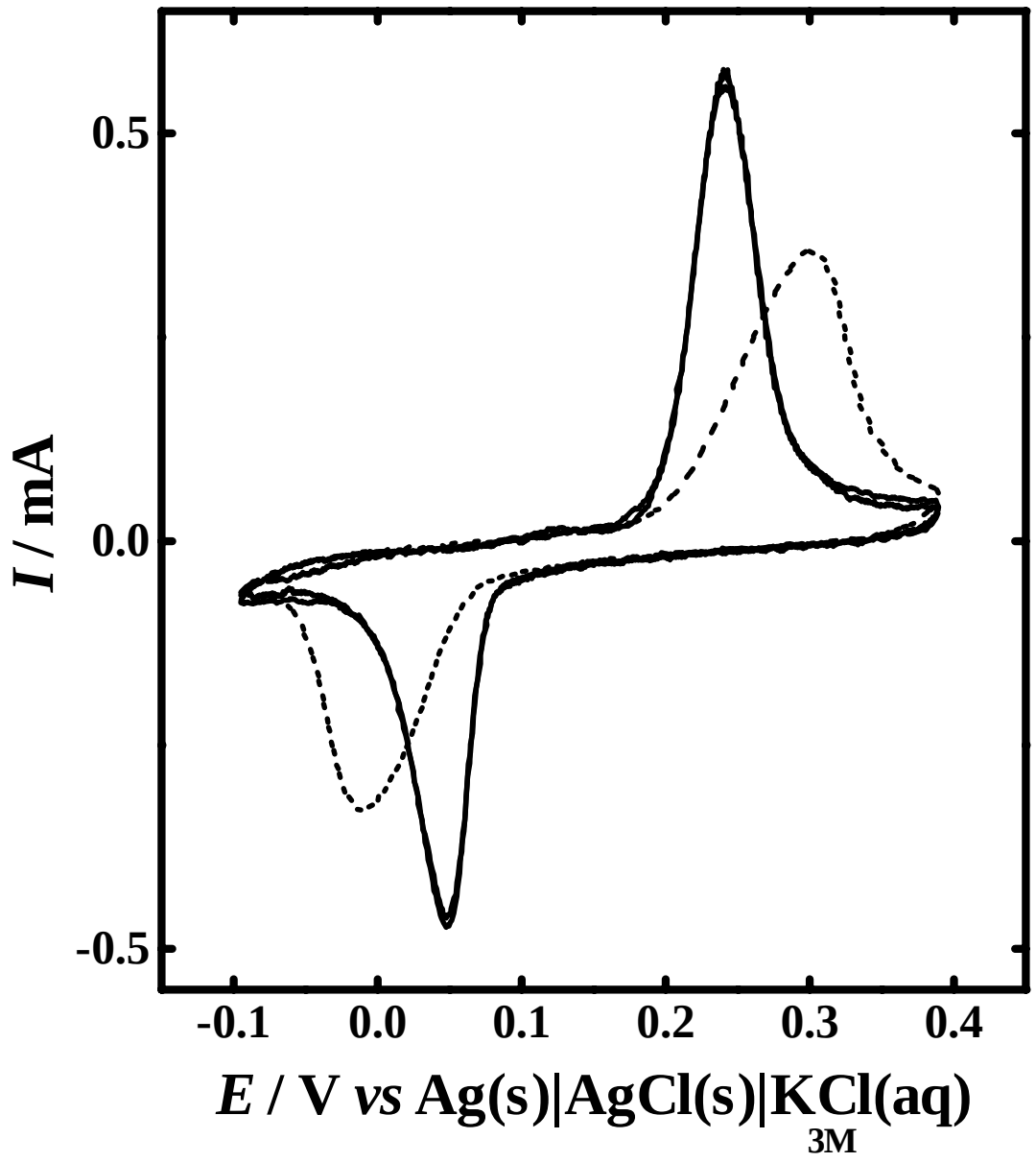

Figure 3.9. Voltammogram of TTF rubbed onto gold quartz crystal in 0.1M KBr(aq) [scan rate of 100 mV s^{-1}]. Solid line is the voltammogram with the reference tip as close as possible to the working electrode. Dotted line is the voltammogram with the reference tip 1 cm away from the working electrode.

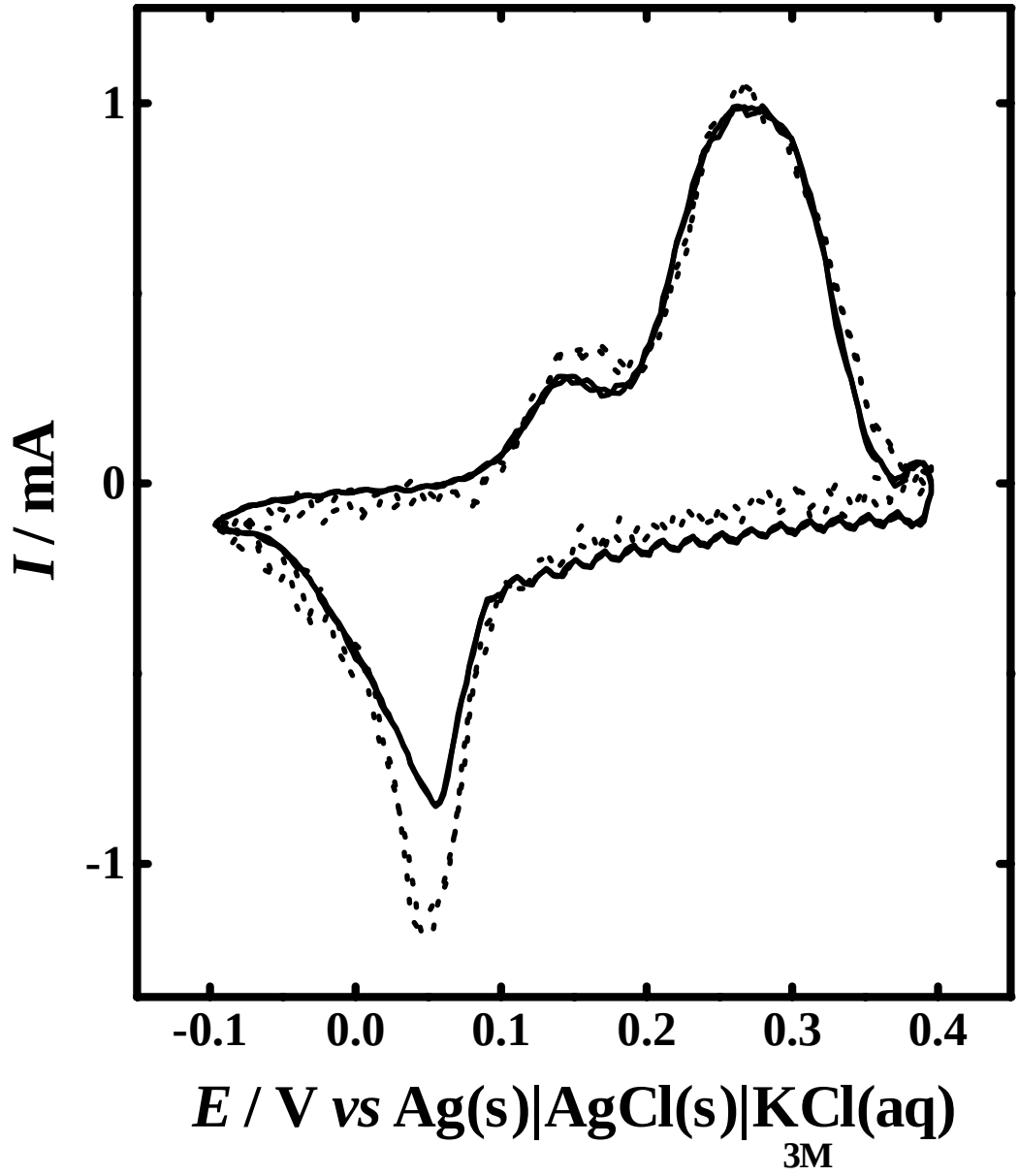

Figure 3.10. Voltammogram of TTF rubbed onto gold quartz crystal in 0.1M KBr(aq) [scan rate of 1000 mV s^{-1}]. Solid line is the voltammogram and dotted line is massogram scaled to the current.

shows the massogram scaled to the voltammogram for the oxidation of TTF. The fact that there is no distortion in peak shape demonstrates that scan rates of at least 1000 mV s^{-1} can in fact be used. Thus in these studies the upper limit of scan rate used was 1000 mV s^{-1}.

3.3.2.5. Temperature Dependence.

The quartz crystal's frequency is linearly dependent on temperature [15-18]. Although this has enabled its use as a temperature sensor in NMR measurements, the temperature dependence also means that frequency drifts can occur as a result of temperature drifts of the order of a fraction of a degree as can occur during solution equilibration. Although the laboratory in which the experiments were conducted was airconditioned (temperature controlled), small variations in temperature were unavoidable in an unthermostated cell. Nonetheless, this was not a problem when working in the microgram region.

3.3.2.6. Noise.

The inherently vibrating nature of the quartz crystal microbalance means that the electrochemical data obtained will be significantly noisier than that obtained from a conventional stationary voltammetric configuration. Furthermore, the instrument must separate the electrochemical signal from a higher frequency (10 MHz) excitation signal, which further increases the noise sensitivity inherent in the QCM design. For this reason, the electrochemical experiments not requiring the

measurement of mass deposition would be better conducted with a conventional electrochemical cell setup.

3.4. References.

[1] Sauerbrey, G., *Z. Physik,* **1959,** 155, 206-222

[2] Brukenstein, S.; Shay, M., *Electrochimica Acta,* **1985,** 30(10), 1295-1300

[3] Elechema, *Technical Manual: Electrochemical Quartz Crystal Nanobalance,* 17

[4] Gabrielli, C.; Keddam, M.; Torresi, R., *J. Electrochem. Soc.* **1991**, 138(9), 2657-2660

[5] Brukenstein, S.; Swathirajan, S., *Electrochimica Acta,* **1985,** 30(7), 851-855

[6] Borges, G.L.; Kanazawa, K.K.; Gordon, J.G.; Ashley, K.; Richer, J., *J. Electroanal. Chem.*, **1994,** 364, 281-285

[7] S. Fletcher, C.S.Halliday, D. Gates, M. Westcott, T. Lwin and G.Nelson, *J Electroanal. Chem.*, **1983,** 159, 267-285

[8] Dean, J.A., *Langes Handbook of Chemistry*, McGraw-Hill Book Company: Sydney, **1985**, 6-2 to 6-4.

[9] Gu, N.; Niu, L.; Dong, S., *Electrochem. Comm.*, **2000,** 2, 48-50

[10] Deakin, M.R.; Melroy, O., *J. Electroanal. Chem.*¸**1998,** 239, 323-331

[11] Arrigan, D.W.M.; Bihan, L.L.; Pickup, M.J., *The Analyst*, **1999,** 124, 1797-1802

[12] Wilde, C.P.; Zhang, M., *J. Electroanal. Chem.*, **1992,** 338, 359-365

[13] Hillier, A.C.; Ward, M.D., *Anal. Chem.*, **1992,** 64, 2539

[14] Kadish, K.M.; Ding, J.Q.; Malinski, T., *Anal. Chem.* **1984,** 56, 1741-1744

[15] Kampik, M.; Klonz, M.; Skubis, T., *IEEE Transactions on Instrumentation and Measurement*, **1997,** 46(2), 387-390

[16] Yao, S.Z.; Chen, J.H.; Nie, L.H., *Corrosion*, 53(3)**,** 1961

[17] Wang, D.; Leigh, J.S., *J. Magn. Reson. Series B.*, **1994,** 105, 25-30

[18] Simon, G., *J. Magn. Reson.*, **1997,** 128, 194-198